

9 Framework automated tuning

The models and algorithms from Chapter 6 constitute the basis for the radio-coverage framework used throughout this thesis. Until here, the framework has been studied in the context of optimization-problem solving for radio networks. In this chapter, the focus is shifted towards radio-network planning activities, and how the framework can aid a network-planning engineer in his or her everyday tasks. The objective is to facilitate refined network planning, the complexity of which is generally beyond the scope of any manual approach.

A central part of a radio-planning tool is its radio-propagation model. Generally speaking, the signal-propagation predictions will be as good as the input data used for their estimation. Moreover, acquiring and constantly upgrading the necessary data to support the decision making in this context is an expensive and challenging task. In practical situations, an emitted signal propagates by interacting with the surrounding environments. Consequently, the ability of a propagation model to adapt to the environment where it is used improves the accuracy of the calculated signal-propagation predictions.

In this context, this chapter presents two automated-tuning capabilities for PRATO. The first one involves the parameter tuning of the empirical radio-propagation model using a snapshot of field measurements. The second one involves the optimization of clutter losses over different regions of the country, therefore adapting the loss factors to the local conditions of each region. The results of the experimental simulations, performed over three regions of the real LTE network deployed by Telekom Slovenije, d.d., show the suitability of the presented methods to improve the accuracy of the calculated radio-propagation predictions.

To the best of the author's knowledge, there is no reference in the literature of an optimization-based approach to automatically adapt the signal losses due to clutter. The content of this chapter extends the research work published by the author in [22].

The rest of this chapter is organized as follows. Section 9.1 describes the benefits of the presented approach from the radio-planning point of view. After giving an overview of relevant publications in Section 9.2, the parameter-tuning problem and the analytical approach for solving it are presented in Section 9.3, including the experimental simulations and their results. Section 9.4 concentrates on the description of the optimization problem involving the regional adaptation of signal losses due to clutter, including an extensive analysis of the performed simulations on three test networks.

9.1 Motivation

With the advent of LTE as part of the 4G in cellular technology, mobile operators are facing the challenges of deploying a new network. LTE follows the well established UMTS/HSPA combo, targeting higher peak data rates, higher spectral efficiency and lower latency [149].

The deployment of a new radio network is always a challenge for mobile operators, who constantly struggle to find the optimal investment in order to provide a competitive network in terms of coverage and QoS. Indeed, coverage planning remains a key problem that all operators have to deal with.

Although different mathematical models have been proposed for radio-propagation modeling, none of them excels in a network-wide scenario [137]. Empirical propagation models usually give good results with a limited computational effort. However, for improved accuracy, the model parameters have to conform to a specific network or region within it, mainly because of the inaccuracies in input data and the environmental changes in the region, e.g., foliage of trees or snow. Consequently, a combination of different parameters is generally needed in order to reliably calculate radio-propagation predictions of lar networks that cover different environments.

To address the afore-mentioned issues, the parameters of an empirical propagation model are adapted based on a set of field measurements. The parameter tuning is analytically calculated per cell, in order to increase the accuracy of the calculated predictions. Moreover, by applying an optimization approach, the signal losses due to clutter are automatically adjusted in a regional basis.

As a simulation framework to evaluate the presented problems, PRATO, the parallel radio-prediction tool presented in Chapter 6, is used. Therefore, the suitability of the framework for network planning and optimization of LTE radio networks is also validated. Specifically, the tool should be capable of handling a large number of radio-propagation predictions using a metaheuristic algorithm, and a distributed objective-function evaluation.

9.2 Related work

Following an optimization-oriented approach, the authors of [3] study the effects on location accuracy while performing semi-automated optimization of the parameters of a radio-propagation model. While their optimization component improves the accuracy of the radio predictions, it does so requiring human intervention, hence the term semi-automated optimization. In terms of the effects of location accuracy, they conclude that locations with a median accuracy of around 60 m may be used for parameter tuning. Also, they notice that although the model accuracy improved after the parameter tuning, it gives inadequate results when used for predicting radio propagation over distant areas.

<More related work, ???>

je cestasť?

9.3 Parameter tuning of the radio-propagation model

The effectiveness of the decision-making process during radio-network planning is tightly coupled with the precision achieved by the propagation model used. In order to obtain a radio-propagation model that most accurately reflects the propagation characteristics of the area covered by each radio cell in the network, the parameters of the mathematical model are adapted to the target environment into which it is to be used. Current state-of-the-art methods for such parameter tuning depend on existing field-measurement data [3, 178], which are collected in advance for the area covered by the target network. Starting from an a-priori best-known set of parameters, empirically calculated by the radio engineers, this approach adapts the model parameters so that the deviation of the radio-propagation prediction to a given set of field measurements is minimized.

To calculate the radio-propagation predictions, the empirical model, previously introduced in Section 6.3.2, ~~Chapter 6~~, is used. Recall that the model contains a vector of adaptable parameters, β . For this reason, this mathematical model is especially appropriate for tuning, since it can be adapted to a given scenario and its local conditions by adjusting the values of the vector $\beta = (a_0, a_1, a_2, a_3)$, the elements of which represent:

a_0 the reference loss or offset,

*INÉ VĒKTORU ĢĒ STĀNDARDO
OZNĀCĒ, KODI "MOLD" ALI S " "
VELIA ZA 'POVON V TEKSTU*

Table 9.1: Clutter-category label numbers and descriptions for the signal loss due to clutter, as reflected by a radio-propagation model.

Clutter category	Description
0	Urban area without buildings, mostly roads
1	Suburban area
2	Urban area
3	Dense urban area
4	Agricultural area
5	Forestall area
6	Swamp area
7	Dry open land area with special vegetation
8	Dry open land area without special vegetation
9	Water area
10	Industrial area
11	Park area



- β_1 the loss slope due to distance of the receiver from the transmitter,
- β_2 the loss slope due to height of the transmitter antenna, *and* ?? *(konsistenz)*
- β_3 the loss slope due to the combined effect of the distance and height of the antenna.

The parameter tuning is performed per cell to improve the local fitting of the radio predictions, being its resulting solution a vector β_c for a target cell c , $c \in C$.

Also, recall that the model includes an extra term in order to adequately predict signal-loss effects due to foliage, buildings and other fabricated structures. These loss factors are based on the land usage, known as clutter data. Here, twelve different clutter categories are recognized. Table 9.1 lists these categories, including their label numbers and descriptions.

9.3.1 Field measurements

In radio networks, an UE constantly performs cell selection/reselection procedures and handover (see Section 3.1, ~~Chapter 3~~), in order to keep the best possible connection to the network. Within this context, the best connection is selected by probing a QoS measure of the neighboring cells. In LTE networks, the UE measures two parameters from the reference signal of the network, namely the Reference Signal Received Power (RSRP) and the Reference Signal Received Quality (RSRQ).

For a certain frequency bandwidth, RSRP measures the average received power over the resource elements that carry cell-specific reference signals. RSRP is applicable in both idle mode (e.g., waiting for a call) and connected mode (e.g., during a call). During the procedure of cell selection/reselection in idle mode, RSRP is used, whereas RSRQ is only applicable when the UE is in connected mode.

The radio-propagation prediction involves calculating the network coverage over a certain region. Hence, in the first place, the focus is on accurately predicting the best connection an UE would select in idle mode and the RSRP measurements it uses.

Here, the field measurements representing the RSRP at a given location were collected using a small truck, that was equipped with a spectrum analyzer. The spectrum analyzer was connected to an external omni antenna mounted on the roof of the truck, at roughly 2 m above the ground, taking measurements at a rate of 2 Hz. To accurately establish the measurement-location points, a GPS unit was used. These GPS-informed locations have

~~✓~~

KONSISTENZ

been tested to be compliant with the 60m limit mentioned in [3]. The measurements cover most of the streets within the target area, with over 300,000 individual points, collected for more than 140 network cells.

To minimize the error impact in measured RSRP, all field measurements are processed so that a single value, the median, was calculated for each of the measured locations. This processing step improves measured-data quality in terms of possible deviations due to external factors, e.g., driving speed. The resulting RSRP was then used to estimate the path-loss prediction at the corresponding location, the resolution of which matches that of the DEM and clutter data used.

9.3.2 Linear least squares

The approach for tailoring the radio-prediction model is to correlate the field measurements with the predicted RSRP values. The new parameter set originates from the minimization of an error criterion. Similar to [3, 83, 178], the minimization criterion is the squared-sum difference between the predicted and the observed RSRP levels, i.e.:

$$E(\beta_c) = \sum_{i=1}^{m_c} (p_c - pl_c(i, \beta_c) - fm_i)^2, \quad (9.1)$$

where $E(\beta_c)$ is the observed error for cell c given the parameters β_c , p_c is the pilot power of cell c , and $pl_c(i, \beta_c)$ is the path loss of cell c at the same geographical point of fm_i , i.e., the i -th field measurement out of a set of measurements for cell c , the cardinality of which is m_c .

A necessary condition for the linear least-squares method to find the global minimum is the linear relationship between the predicted path loss, $pl_c(i, \beta)$, and the vector β_c [178]. This condition can be verified by calculating the first derivative of $E(\beta_c)$ in terms of the components of vector $\beta_c = \langle \beta_{0c}, \beta_{1c}, \beta_{2c}, \beta_{3c} \rangle$, i.e., $\frac{\partial E(\beta_c)}{\partial \beta_{0c}} = 0$, $\frac{\partial E(\beta_c)}{\partial \beta_{1c}} = 0$, $\frac{\partial E(\beta_c)}{\partial \beta_{2c}} = 0$, and $\frac{\partial E(\beta_c)}{\partial \beta_{3c}} = 0$.

9.3.3 Simulations

The simulations consisted in building the matrices of the observed-error values, $E(\beta_c)$, for each cell c in the target network. The linear systems of equations are then individually solved by applying the linear least-squares method, which involves the evaluation of one radio-coverage prediction per cell. Each solved system holds a unique solution for a cell c , $c \in C$, denoted by the vector β_c .

9.3.4 Test networks

The test networks, Net₈, Net₉, and Net₁₀, are subsets of a real LTE network deployed in Slovenia by Telekom Slovenije, d.d. The path-loss predictions are calculated using PRATO, with a DEM and clutter map of 25 m² resolution, and a receiver height of 2 m above ground level. A transmission radius of 16 km defines the coverage prediction area around each network transmitter, thus limiting the path-loss prediction to a distance where it is feasible for an UE to connect to a cell, with a RSRP greater or equal to -124 dBm [115]. At the same time, the selected transmission radius provides enough overlap among neighboring cells to calculate the network coverage over the whole region. Table 9.2 provides detailed information about the test networks used, showing the number of network cells, the area surface, and the covering proportion of the collected field measurements in terms of the total area of each test network.

Table 9.2: Several properties of the test networks Net_8 , Net_9 and Net_{10} , that were used for the experimental simulations during the automated tuning of the radio-propagation model.

	Number of cells	Area [km ²]	Field-measurement proportion [%]
Net_8	12	103.74	5.41
Net_9	130	1298.02	12.02
Net_{10}	6	386.38	2.30

Table 9.3: Clutter-category proportions, expressed in percent, in terms of the surface area of each of the test networks. The category legend is given in Table 9.1.

	Cat.0	Cat.1	Cat.2	Cat.3	Cat.4	Cat.5	Cat.6	Cat.7	Cat.8	Cat.9	Cat.10	Cat.11	Total
Net_8	0.53	4.53	1.68	0.45	71.89	17.94	0.07	0.00	0.03	2.21	0.67	0.00	100.00
Net_9	0.91	5.53	9.48	3.84	29.73	48.57	0.14	0.03	0.03	0.76	0.86	0.12	100.00
Net_{10}	0.15	3.99	1.14	0.11	26.50	67.13	0.26	0.00	0.00	0.36	0.36	0.00	100.00

Net_8 represents a network deployed over a dominant agricultural area with almost flat terrain, some forests and water streams. Net_9 is deployed over a densely populated urban area, containing high buildings, parks and avenues. The last one, Net_{10} , represents a network deployed over hilly terrain, including some smaller villages and vast forests. It is important to note that the number of deployed cells is directly proportional to the population density within the region of each test network (see Chapter 3). This relationship can be derived from the information listed in Table 9.2, where the number of cells is shown along the area of every test network. For a clearer characterization in terms of the terrain types and their extent, the proportion of each clutter category with respect to the total area of every test network is shown in Table 9.3.

The terrain profiles are most relevant for Net_8 and Net_{10} , since none of them contains densely populated urban areas. Note that the terrain shown in Figure 9.1 is mostly flat, since the agricultural area prevails in Net_8 . In contrast, the terrain for Net_{10} is dominated by hills, which are mostly covered by dense forests, including some small villages in the valleys (see Figure 9.2).

In the following, the default parameters of the radio-propagation model correspond to the values provided by the engineers of the Radio Network department at Telekom Slovenije, d.d.

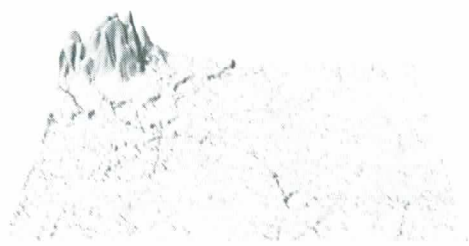


Figure 9.1: Terrain profile of the test network Net_8 , dominated by a flat agricultural area.

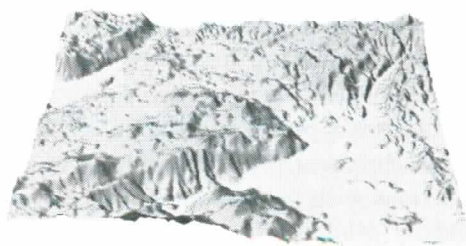


Figure 9.2: Terrain profile of the test network Net_{10} , dominated by forested hills.

ZAKAS NI ŠE NAREŠENO (SLIKA + OVIS) EA
NET₉!

9.3.5 Experimental environment

The simulations were carried out on several computing nodes of the previously presented DEGIMA cluster [72] at the NACC of the Nagasaki University in Japan (see Section 6.5, ~~Chapter 6~~). Groups of 3, 4, and 34 nodes were used for executing the simulations of the different problem instances, i.e., Net₈, Net₉ and Net₁₀, respectively.

9.3.6 Results

The results of applying the linear least-squares method to fit the parameters of the radio-propagation model to a set of field measurements are presented in this section. Bar charts were prepared to show the cumulative distribution of the absolute error between the radio-propagation prediction and the field measurements (see Figures 9.3, 9.4, and 9.5). Each bar represents an open interval, expressed in dB, denoting the proportion of points that deviate from the prediction in the given number of dB. For example, in Figure 9.3 (a), it can be observed that the proportion of predicted points differing from the field measurements in 35 dB or more is around 16%, whereas the proportion of points differing in less than 5 dB is 10%. These values correspond to the test network Net₈, before applying the model-parameter fitting. For comparison, in Figure 9.3 (b), the absolute-error distribution for the same test network is given, but with the model parameters fitted to the available field measurements. Notice how the proportions describing the biggest deviation have dropped to under 5% (35 dB and more), and to less than 6% (30 dB to 35 dB), respectively. Moreover, it is clear how all proportions improved, raising the bars towards the left-hand side of the chart and lowering them on the right-hand side.

The error distributions of the radio-propagation prediction for test network Net₉ using the default parameters and the fitted ones are given in Figures 9.4 (a) and 9.4 (b), respectively. In this case, the improvement is even more significant than for the previous test network, clearly showing that the tuned propagation model represents the local radio-propagation conditions more accurately than the default parameter set.

For the last test network, Net₁₀, the error distributions are depicted in Figure 9.5 (a) using the default parameters, and Figure 9.5 (b) for the tuned ones. Similar to the test network Net₈, it can be clearly seen how the proportions of highest error deviations have been lowered with respect to those with lower deviation values.

The overall results confirm that fitting the parameters of the radio-propagation model to the field measurements of each network cell significantly improves the quality of the calculated radio-propagation predictions. Indeed, since the default parameters were provided by the radio engineers after following a traditional approach for the whole network, it can be concluded that the automated-fitting method is not only simpler and faster, but also superior in terms of solution quality.

However, it is important to note the particular reasons behind the considerable better results for Net₉, when compared to those of Net₈ and Net₁₀. Clearly, the relative quantity of the available field measurements directly affects the quality of the calculated results. Therefore, the least squares approximation is rougher and less precise for the networks where the field-measurement proportion is lower. See Table 9.2 for a reference of the field-measurement proportions with respect to the area surface of each test network. Similar findings were confirmed by other authors, who worked on the adjustment of radio-propagation models to different environments [83]. For the sake of completeness, it is worth pointing out that some researchers have already started working on different ways on how to improve this aspect [115, 116].

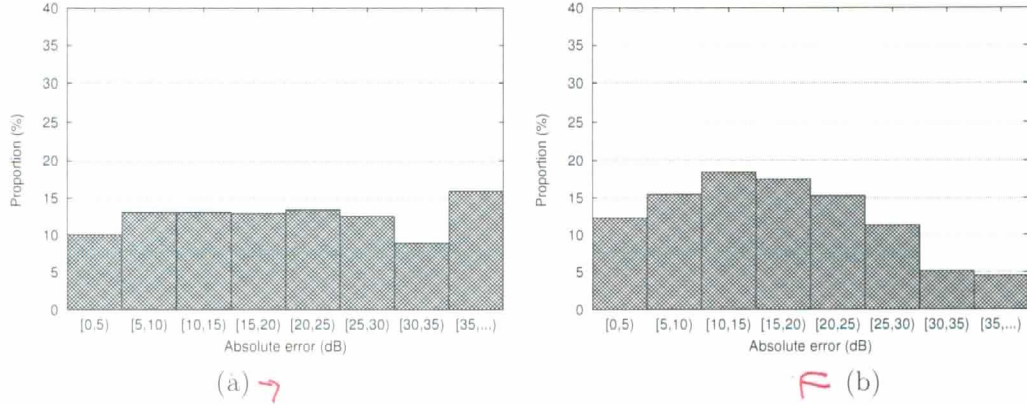


Figure 9.3: Error distribution of the radio prediction for network Net₈: (a) with default parameter values, and (b) with fitted parameter values.

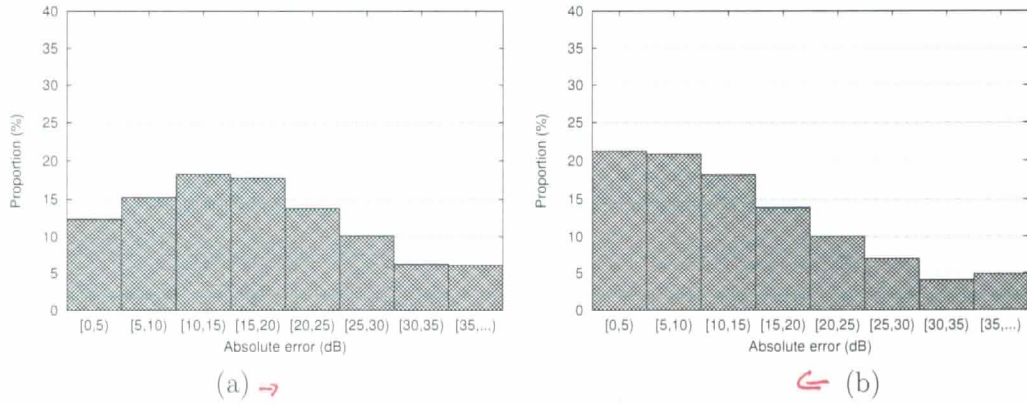


Figure 9.4: Error distribution of the radio prediction for network Net₉: (a) with default parameter values, and (b) with fitted parameter values.

9.4 Clutter optimization

In order to further improve the accuracy of the radio-prediction calculation over a given regional environment, the signal losses due to clutter are optimized in this section.

As it was mentioned before, there are several reasons for the predicted signal-loss values to be inaccurate. The seasonal changes are among them, like tree foliage or snow. Also, changes related to urban development, like demolition or construction of buildings and parks, and different kinds of forests or agricultural areas, etc. These changes are only noticeable through regular updates of accurate land-use data. However, in the short term, updates are only available in the form of feedback by means of field-measurement campaigns.

In the following, a metaheuristic algorithm is used to optimize the clutter losses of several regions within a target radio network. This is done over groups of network cells within different regions of the target network, e.g., agricultural, urban or hilly. In terms of coverage planning, a regional classification of the signal losses due to clutter improves the accuracy of the radio-coverage prediction.

In contrast to the parameter tuning of the mathematical model presented in Section 9.3, an analytical approach is not used for tackling this problem. Instead, the DASA metaheuristic algorithm is the tool of choice for optimizing the clutter losses.

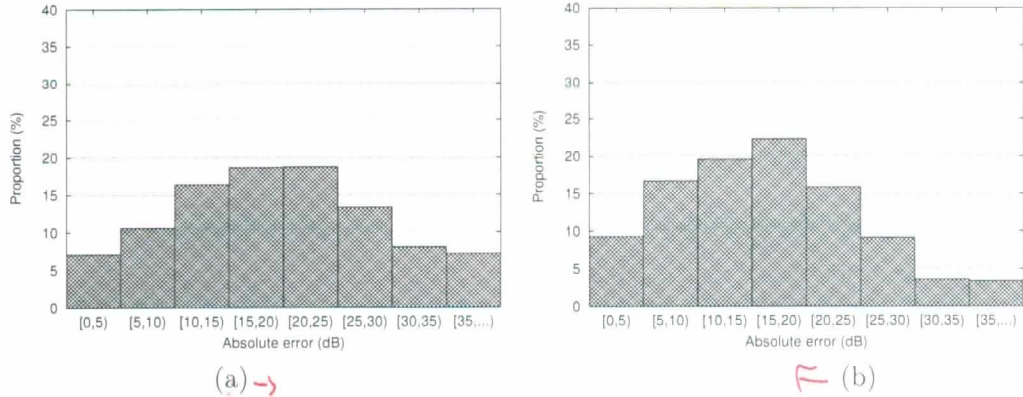


Figure 9.5: Error distribution of the radio prediction for network Net₁₀: (a) with default parameter values, and (b) with fitted parameter values.

There are several reasons for choosing the DASA as the optimization algorithm in the context of this problem. First, the benefits of metaheuristic algorithms for solving optimization problems, particularly in the context of radio networks, was demonstrated by several authors in general [19, 56, 83, 102], and in this thesis in particular (see Chapters 4, 7 and 8). Second, in [92], the authors validated the suitability of the algorithm for solving numerical-optimization problems.

9.4.1 Optimization objective

The optimization objective consists in adjusting the loss values of the different clutter categories, i.e., $pl_{CLUT}(d_{(x,y)})$ from Equation (6.3), Chapter 6, according to a set of field measurements of a given geographical region. The same three data sets used in Section 9.3.3 were used for the clutter-optimization problem: the first for Net₈, the second for Net₉, and the third for Net₁₀. Each region was independently optimized, so that the radio-propagation predictions of each set of network cells minimized the mean-squared error against the field measurements, i.e.:

$$\min f_{clut} = \sum_{i=1}^{m_c} \frac{(p_c - pl_c(i, \beta_c^*) - fm_i)^2}{m_c} \quad \forall c \in C, \quad (9.2)$$

where f_{clut} is the optimization objective to be minimized in each of the three regions, p_c is the transmit power of cell c , fm_i is the i -th field measurement of cell c , the set of which has cardinality m_c , and m_C is the number of field measurements of all the cells of a given network. Similar to the least-squares approach, $pl_c(i, \beta_c^*)$ represents the path loss of cell c at the same geographical point of the i -th field measurement, and β_c^* denotes the fitted parameter values of the prediction model for cell c .

For a reference of the different clutter categories used by the radio-propagation model, see Table 9.1.

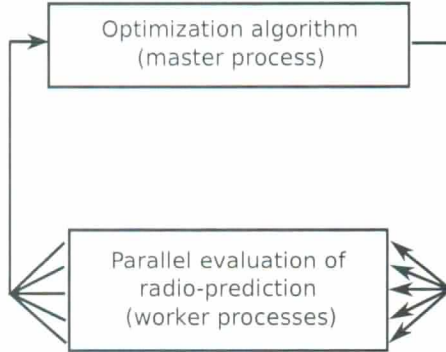


Figure 9.6: Architecture and data flow of PRATO during the clutter-optimization phase. The optimization algorithm runs on the master process, while the radio-propagation predictions of the involved network cells run in parallel over several worker processes.

9.4.2 Differential ant-stigmergy algorithm

The chosen optimization algorithm for the clutter-optimization problem is the DASA (see Section 2.3.2, Chapter 2). The mapping between the clutter-optimization problem and DASA is as follows:

$$X_a = \{x_0, x_1, \dots, x_i, \dots, x_{11}\}, \quad (9.3)$$

where X_a is the solution vector of ant a during the minimization process, and x_i represents the i -th clutter category within a given region or network. At the end of every iteration, and after all the ants have created solutions, they are evaluated to establish if any of them is better than the best solution found so far.

9.4.3 Simulations

In this case, one simulation round consisted of multiple iterations of several steps. An iteration begins by generating a solution vector for each of the ants in the DASA colony. The following step involves the parallel evaluation of the solution vector carried by an ant, i.e., one radio-propagation prediction per worker process. The final step consists in calculating the objective-function value, as defined in Equation (9.2), before sending it back to the master process for the DASA to generate the next set of solutions. Figure 9.6 depicts the way PRATO performs the parallel objective-function evaluation over the worker processes, while the optimization algorithm runs on the master process.

As opposed to the least-squares case, a much larger number of evaluations is needed for this kind of optimization. Therefore, it is essential to exploit the parallel nature of the framework in order to simultaneously evaluate the radio-coverage prediction of multiple cells. Otherwise, a metaheuristic approach would not be feasible, due to the computational time required to reach a reasonable solution.

The default clutter-loss values (expressed in dB) for each clutter category, which are listed in the second column of Table 9.4, were provided by the radio experts of the Radio Network department at Telekom Slovenije, d.d. These values were empirically calculated using a classic (i.e., manual) approach, the results of which are regularly loaded into a commercial radio-planning application in order to validate the radio coverage at a network-wide level. The radio experts also suggested limiting the optimized clutter-loss values to a maximum of 40 dB.

Table 9.4: Clutter-category losses after the optimization. The default losses for each clutter category are given along the solutions for each of the test networks. All values are expressed in dB.

Clutter category	Default	Net ₈	Net ₉	Net ₁₀
0	5.0	13.71	11.30	17.90
1	15.0	12.39	16.67	-
2	13.0	16.04	17.04	15.69
3	28.0	19.59	18.01	23.00
4	12.0	11.48	9.71	10.80
5	20.0	16.26	11.62	16.26
6	15.0	-	-	-
7	8.0	-	13.49	-
8	5.0	-	13.50	-
9	1.0	17.50	5.60	-
10	20.0	8.26	16.75	16.63
11	8.0	-	18.93	-

SET BY

The stopping criteria for the optimization runs was setting the maximum allowed number of objective-function evaluations. In this sense, the limits for Net₈ and Net₁₀ were set the 200, whereas for Net₉ the value was 500, since this network contains the largest number of cells. Overall, the framework completed 48,000 objective-function evaluations, i.e., 576,000 radio-coverage predictions for Net₈ and 288,000 for Net₁₀, whereas for Net₉, the number of objective-function evaluations was 120,000, for a total of 15,600,000 radio-coverage predictions.

Regarding the parameters that control the behavior of the DASA, they were set to the following values:

- $m = 240$, the number of ants;
- $b = 10$, the discrete base;
- $q = 0.2$, the pheromone dispersion factor;
- $s_+ = 0.01$, the global scale-increasing factor;
- $s_- = 0.01$, the global scale-decreasing factor; and
- $e = 1.0^{-2}$, the maximum parameter precision.

HOW WHERE THEY SET!?)

9.4.4 Results

The results achieved by the optimization process are shown in Table 9.4. The solutions are given for each of the test networks, along with the empirically-calculated (default) loss values. Hyphens represent clutter categories for which there were no field measurements available. Consequently, it was not possible to evaluate the objective-function for them.

The optimized loss for the first clutter category, 0, representing urban area without buildings, is larger than the default value in all three networks. This may be attributed to the fact that these areas are not completely open, mostly surrounded by forests (Net₈ and Net₁₀) and buildings of different sizes (Net₉). As for the category 1, representing suburban area, the value for Net₈ is lower than the default one, mainly because this network is deployed over a predominant agricultural area, i.e., suburban areas are less dense here. On the other

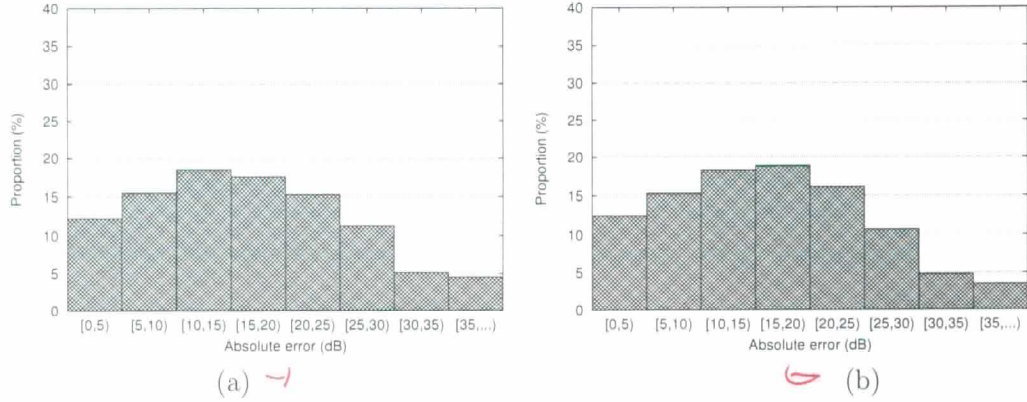


Figure 9.7: Error distribution of the radio prediction for network Net8: (a) with fitted parameter values and default clutter losses, and (b) with fitted parameter values and optimized clutter losses.

hand, the value for Net₉ is larger, indicating a building density above the average, whereas for Net₁₀, the value could not be calculated due to the lack of measurements. For the category 2, representing urban area, the optimized values are above the default ones, clearly showing an underestimation of the manual approach. However, there is a relation among the clutter losses that corresponds to the population density in each of the regions, being Net₁₀ the less dense urban area among the three networks. The optimized values of the category 3, representing dense urban area, are lower than the default ones. This indicates that the dense urban areas in these regions have a lower density than the average case. Representing the agricultural area, the category 4 gets a value very close to the default one for Net₈ and Net₁₀, whereas for Net₉ the value is lower, indicating that this type of land is mostly open near the city, e.g., without plantations. As for the category 5, representing forests, the results correspond with the type of forest that dominates each of the test-network regions. Namely, Net₈ and Net₁₀ are dominated by dense forests presenting leave foliage, whereas in Net₉ the forests are mostly coniferous and more sparse. Keeping most of the default loss values for the categories 6, 7 and 8, the results of the next category, 9, representing water, indicate creeks and rivers in these areas are almost entirely surrounded by forests (Net₈) or buildings (Net₉), since none of the regions lays by the sea. As for the industrial area, denoted by the clutter category 10, lower loss values than the empirically-calculated defaults appear. This indicates the presence of sparse industrial buildings in Net₈, and a higher density of mostly commercial buildings for Net₉ and Net₁₀. The last clutter category, 11, could not be calculated for Net₈ and Net₁₀ due to the lack of field measurements.

Notice that the relation among the different clutter categories is correctly kept for the three test networks. For example, it can be observed that the clutter loss for dense urban area (category 3) is higher than the values of the urban area (category 2), as well as of the agricultural area (category 4). Hence, the results reflect physically feasible losses, despite the higher deviation from the default losses shown by the category 2, and the lower deviation for the category 3, again with respect to the default losses. Such relations hold for different categories of all three test networks, strongly suggesting the correctness of the applied optimization approach and the evaluation methodology used. Consequently, it can be confirmed that the combination of PRATO and a metaheuristic algorithm is applicable for performing the automatic adjustment of clutter losses, since it is capable of reflecting the physical phenomena appearing in real-world conditions and improving the quality of radio-propagation predictions for three, geographically different, radio-network instances.

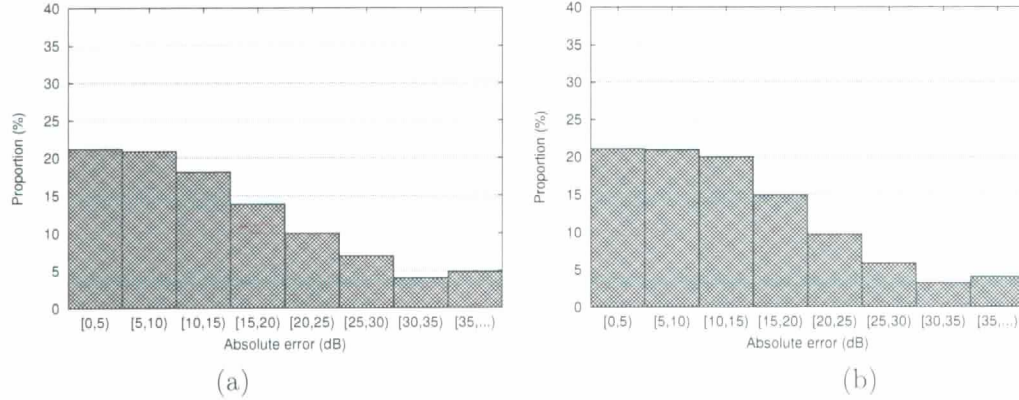


Figure 9.8: Error distribution of the radio prediction for network Net₉: (a) with fitted parameter values and default clutter losses, and (b) with fitted parameter values and optimized clutter losses.

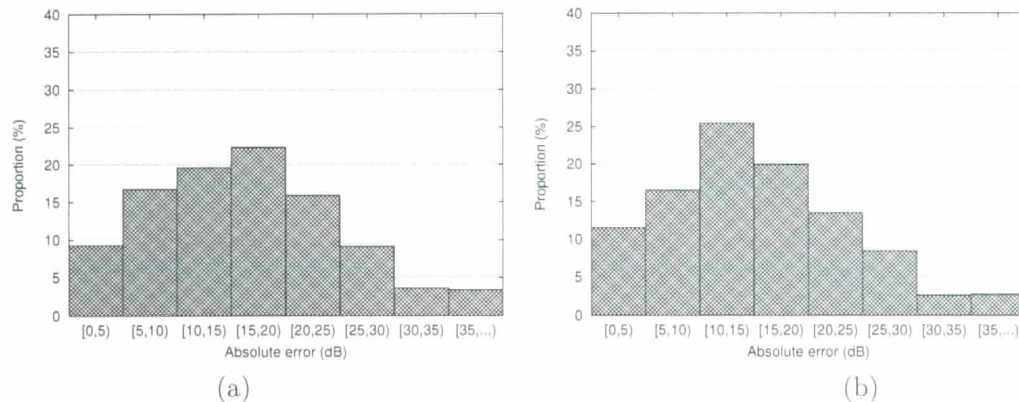


Figure 9.9: Error distribution of the radio prediction for network Net₁₀: (a) with fitted parameter values and default clutter losses, and (b) with fitted parameter values and optimized clutter losses.

Table 9.5: Statistical analysis of the solutions for the clutter-optimization problem. All values are expressed in dB. The corresponding box plots are depicted in Figure 9.10.

Cat.	Nets ₈					Net ₉					Net ₁₀			
	Min	Max	Avg	St.dev.		Min	Max	Avg	St.dev.		Min	Max	Avg	St.dev.
0	13.36	13.97	13.71	0.15		11.22	11.40	11.30	0.04		17.72	17.85	17.90	0.07
1	-	-	-	-	-	14.25	19.20	16.67	1.87	-	-	-	-	-
2	15.84	16.21	16.04	0.08		16.99	17.11	17.04	0.03		15.64	15.72	15.69	0.03
3	19.15	20.07	19.59	0.25		17.95	18.12	18.01	0.04		22.68	23.20	23.00	0.16
4	11.35	11.62	11.48	0.05		9.63	9.77	9.71	0.03		10.73	10.84	10.80	0.03
5	16.00	16.54	16.26	0.14		11.45	11.80	11.62	0.08		16.19	16.30	16.26	0.04
6	-	-	-	-	-	-	-	-	-	-	-	-	-	-
7	-	-	-	-	-	12.71	14.52	13.49	0.39	-	-	-	-	-
8	-	-	-	-	-	12.25	15.79	13.50	0.83	-	-	-	-	-
9	16.07	18.80	17.50	0.83		4.67	6.26	5.60	0.35	-	-	-	-	-
10	7.79	8.54	8.26	0.19		16.68	16.87	16.75	0.05		16.50	16.68	16.63	0.07
11	-	-	-	-	-	18.62	19.20	17.04	0.13	-	-	-	-	-

Similar to Section 9.3.6, bar charts show the cumulative distribution of the absolute error between the signal-propagation prediction and the field measurements (see Figures 9.7, 9.8, and 9.9). Figure 9.7 (a) depicts the error distribution of the prediction for test network Nets using the fitted model parameters, whereas Figure 9.7 (b) shows the absolute-error distribution for the same test network, but using the optimized clutter losses (see Table 9.4, column Nets₈). Notice how the error distributions show an improvement when the optimized clutter losses are used, lowering the biggest (right-most) deviations even further.

The error distributions of the radio-propagation predictions for test network Net₉ using fitted parameters and default clutter losses, and fitted parameters with optimized clutter losses, are shown in Figures 9.8 (a) and 9.8 (b), respectively. Similar to Net₈, the improvement appears in the biggest deviations, since their values are lower than when using the default clutter losses.

For the last test network, Net₁₀, the error distributions are depicted in Figure 9.9 (a) using the default clutter losses, and Figure 9.9 (b) for the optimized ones. Again, the fitted model parameters were used for both simulation sets. In this case, a more significant improvement than for the other two networks appears, clearly showing the favorable effect of the optimization process. Moreover, this result suggests that some of the default clutter losses considerably fail in representing the actual physical conditions in the geographical region of this network.

Overall, the presented results confirm that the optimization of clutter losses with respect to field measurements improves the quality of the calculated radio-propagation predictions. Considering the default clutter losses were empirically calculated by the radio engineers for the whole network, the convenience of the automated optimization procedure is clear. Indeed, these advantages are a consequence of a simpler method that automatically delivers radio-predictions of superior quality, thus accurately representing the physical properties of a given environment.

Because of the stochastic nature of the DASA, the results of 30 independent runs were collected in order to have enough data for them to be statistically relevant. In other words, the robustness of the solutions, that have been presented in the previous section, is analyzed here.

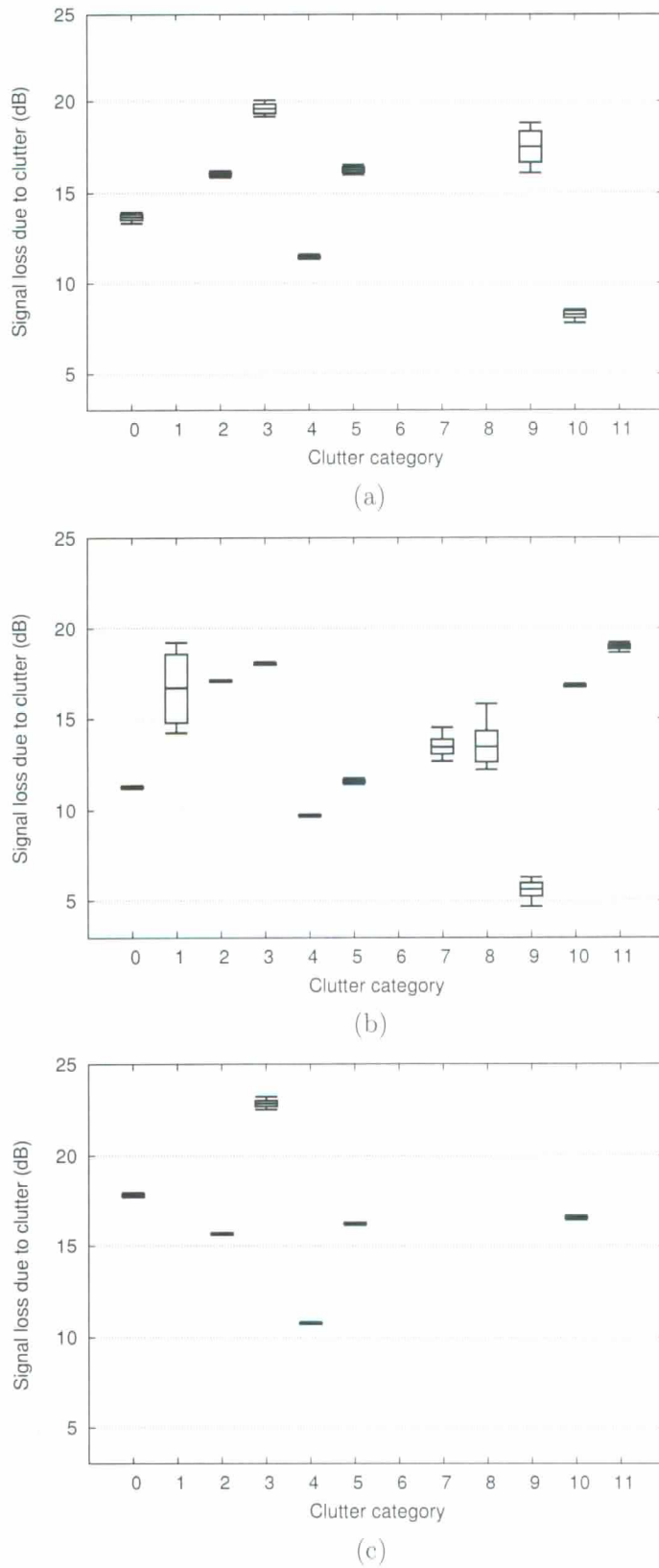


Figure 9.10: Box plots representing the statistical-analysis values of Table 9.5, for the solutions of the clutter-optimization process of each test network: (a) Net₈, (b) Net₉, and (c) Net₁₀.

To this end, Table 9.5 shows the solutions reached by the DASA for each of three test networks. The calculated signal losses are depicted with the minimum, maximum and average values for every clutter category, along with their standard deviations. Again, hyphens represent clutter categories for which there were no field measurements available, and thus they could not be optimized. In order to easily visualize the data shown in Table 9.5, box plots based on the same values are provided in Figure 9.10. It can be observed that the standard deviation is low for almost all optimized categories, indicating a consistent convergence of the optimization algorithm. However, some exceptions are noticeable, e.g., the category 9 in Net₈ and Net₉, representing water. In this case, there was a significantly lower density of field measurements nearby water trails, since none of the test networks lays by the sea. Regarding the categories 1 (suburban area), 7 and 8 (dry open land area) of Net₉, a lower proportion of field measurements over these areas was indentified, thus higher standard-deviation values appear.

Based on these findings, the standard deviation of the optimized clutter losses can be considered an indicator of the field measurements required by the optimization process, i.e., a higher standard deviation denotes more field measurements are needed to optimize the target clutter category.

9.5 Summary

This chapter illustrated the suitability of PRATO as a network-planning tool by tackling two coverage-planning problems, which were tested over the newly deployed LTE network in Slovenia. The first one involved the parameter tuning of the empirical radio-propagation model using a snapshot of field measurements. The second one considered the optimization of the clutter losses over different regions of the country, therefore automatically adapting them to the local conditions of the geographical region of each network.

The combination of the afore-mentioned techniques with PRATO provides an environment-adaptable framework for radio-network planning. This delivers a tool with a considerable improvement of the solution accuracy of the analyzed instances, especially if compared to traditional, i.e., manual or semi-automated, coverage-planning methods.

Additionally, the simulation results indicate that PRATO is applicable for planning and optimization of real-world radio networks, since it is capable of simulating a large number of coverage configurations in a feasible amount of time. In particular, several of the presented instances show a large computational-time complexity, which is beyond reach for a serial implementation of an automated approach. Moreover, the parallelization capabilities provided by the framework create new problem-solving possibilities, together with the automation of tasks, that have been traditionally done manually by the network engineers. Furthermore, even computational-intensive tasks such as objective-function evaluations for stochastic optimization are feasible if PRATO is used.

KAJ NOVOSTI ??
KOT PRI 6 IN 7